
This is an electronic reprint of the original article.
This reprint may differ from the original in pagination and typographic detail.

Mekgwe, Gadifele Nicolene; Akinribide, Ojo Jeremiah; Akinwamide, Samuel Olukayode; Olorundaisi, Emmanuel; Gonya, Elvis Mdu; Olubambi, Peter Apata

Tribological properties of graphitized TiC_{0.5}N_{0.5} based composites using response surface methodology

Published in:
Tribology International

DOI:
[10.1016/j.triboint.2024.109966](https://doi.org/10.1016/j.triboint.2024.109966)

Published: 01/11/2024

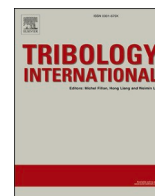
Document Version
Publisher's PDF, also known as Version of record

Published under the following license:
CC BY

Please cite the original version:

Mekgwe, G. N., Akinribide, O. J., Akinwamide, S. O., Olorundaisi, E., Gonya, E. M., & Olubambi, P. A. (2024). Tribological properties of graphitized TiC_{0.5}N_{0.5} based composites using response surface methodology. *Tribology International*, 199, 1-12. Article 109966. <https://doi.org/10.1016/j.triboint.2024.109966>

This material is protected by copyright and other intellectual property rights, and duplication or sale of all or part of any of the repository collections is not permitted, except that material may be duplicated by you for your research use or educational purposes in electronic or print form. You must obtain permission for any other use. Electronic or print copies may not be offered, whether for sale or otherwise to anyone who is not an authorised user.



Tribological properties of graphitized $\text{TiC}_{0.5}\text{N}_{0.5}$ based composites using response surface methodology

Gadifele Nicolene Mekgwe^{a,c}, Ojo Jeremiah Akinribide^a, Samuel Olukayode Akinwamide^{a,b,*}, Emmanuel Olorundaisi^a, Elvis Mdu Gonya^c, Peter Apata Olubambi^a

^a Centre for Nanomechanics and Advanced Materials, School of Mining, Metallurgy and Chemical Engineering, University of Johannesburg, Doornfontein Campus, Johannesburg, South Africa

^b Department of Mechanical Engineering, Aalto University, Espoo, Finland

^c Department of Metallurgy, Faculty of Engineering and the Built Environment, University of Johannesburg, John Orr Building, Johannesburg 2028, South Africa

ARTICLE INFO

Keywords:

Response surface methodology (RSM)
User-defined design
ANOVA
Binderless $\text{TiC}_{0.5}\text{N}_{0.5}$ ceramic composites
Graphite
Wear rate

ABSTRACT

The statistical design of experimental techniques has been widely explored in developing empirical methodologies. These methods are beneficial for developing appropriate mathematical models to predict the properties and performance of various materials. This study utilized the user-defined design (UDD) approach under response surface methodology (RSM) to achieve the optimum parameters for dry sliding wear properties of graphite-reinforced binderless $\text{TiC}_{0.5}\text{N}_{0.5}$ ceramic composites. The tribological tests were performed using a ball-on-flat geometry tribometer, with a ruby- $\text{TiC}_{0.5}\text{N}_{0.5}$ friction pair operating in sliding mode at ambient temperature. The developed mathematical model specifies the functional relationship between the key parameters, using the weight percentage of the graphite reinforcement and applied load as input variables and wear rate as the output variable. Based on the statistical analysis, ANOVA results for wear rate indicated that the predictability of the model is at 95 % confidence level. Moreover, the wear rate demonstrated a correlation coefficient of $R^2 = 0.9762$, which depicts that only less than 3 % of the total variations are not explained by the model, and the value of the adjusted determination coefficient (adjusted $R^2 = 0.9366$) is high, proving that the model is significant.

1. Introduction

Advancements in novel materials extend challenges to manufacturing industries, which compel engineers, scientists, and ceramicists to develop reliable composites in harsh conditions. Cutting tool inserts are necessary to exhibit optimal properties to enhance their performance during milling processes; accuracy and precision are paramount. Wear resistance relies on factors such as type of material, applied load, test speed and time. Ceramic materials possess combined properties such as high hardness, wear resistance and chemical inertness in aggressive environments, making them suitable tools for cutting operations [1] [2]. Due to their superior properties and performance, TiCN-based ceramic composites have successfully substituted WC-Co and TiC cermets in high-speed machining, finishing and semi-finishing of moulds and dies [3] [4] [5] [6].

Wear properties of TiCN-based cermets have been reported in the

literature [7] [8] [7]; however, the performance of this particular class of material depends on several factors such as crystal structure, composition, and experimental conditions (applied load, sliding speed and environment). TiCN has a core-rim structure, the core is the hard phase, and the outer and inner rim constitute a solid solution caused by the reactions between TiCN, binders (Ni/Co/Fe), carbides and nitrides (WC, TiC, TaC, Cr_3C_2 , Mo_2C , TiN, Si_3N_4) particularly used to enhance the properties of the cermets [9] [10] [8] [11]. The interfacial carbon-carbon bonds from carbon-based materials can be incorporated into composite materials to accomplish a lower wear rate due to the passivation at the contact point [12] [13]. Therefore, the intrinsically lubricious property and strong interfacial bonding between graphite and TiCN can improve wear resistance through the load transfer mechanism, promoting solid lubrication and influencing tribo-film formation.

Yadav et al. [14] reported the influence of linear velocity on the sliding wear characteristics of TiCN-based cermets. The sliding

* Corresponding author at: Centre for Nanomechanics and Advanced Materials, School of Mining, Metallurgy and Chemical Engineering, University of Johannesburg, Doornfontein Campus, Johannesburg, South Africa.

E-mail addresses: nicolenemekgwe@gmail.com (G.N. Mekgwe), samuel.akinwamide@aalto.fi, akinwamidekayode@gmail.com (S.O. Akinwamide).

<https://doi.org/10.1016/j.triboint.2024.109966>

Received 8 May 2024; Received in revised form 26 June 2024; Accepted 5 July 2024

Available online 7 July 2024

0301-679X/© 2024 The Author(s). Published by Elsevier Ltd. This is an open access article under the CC BY license (<http://creativecommons.org/licenses/by/4.0/>).

Table 1
Summary of the sliding wear parameters performed on TRB³ tribometer.

Parameters	Value	Units
Linear speed	0.08	cm/s
Acquisition rate	15.0	Hz
Normal load	5, 10 and 20	N
Duration	30	Min
Stop condition	6000	laps

Table 2
Build-up Information for the RSM model.

Software File version: Design expert (13.0.5.0)			
Study type	Response surface	Subtype	Randomized
Design type	User-defined	Runs	9.00
Design Model	Quadratic	Blocks	No Blocks

Table 3
The coded and actual operating conditions of factors.

Independent variables	Units	Coded symbol	Type	Levels	L	L[2]	L[3]
Graphite content	wt%	A	Discrete	3	0	0.5	1.0
Load	N	B	Discrete	3	5	10	20

velocities used were in the range of 0.08 – 0.26 m/s, and at high speed, the cermets showed a higher coefficient of friction (COF), which varied from 0.47 to 0.50 as compared to 0.18 and 0.27 reported for lower velocity. Abrasion, grain pull-out, and adhesion were the dominant wear mechanisms, and the influence of TaC, WC, and Mo₂C was noticeable in the microstructure and mechanical properties, which affected the wear behavior of the material [14]. Stewart et al. [15] investigated the effect of Ni₃Al binder on the wear properties of TiCN cermets using a WC-Co

counterpart using reciprocating test geometry. Cermets with higher binder content showed high COF values (0.45 – 0.52) at lower loads, while at high loads, the specific wear rate and wear track increased. Owing to the limitations caused by the inconsistent microstructures influenced by different materials added to the TiCN hard phase, binderless TiCN composites are used to mitigate the challenges inflicted by the binders [16] [17] [18].

Numerous models can be used to predict the preferred output variables by developing mathematical models that represent the relationship between the input parameters and output variables with minimal experiments. RSM utilizes statistical and mathematical methods that are used for modelling the functional relation between input and output responses of various processes [19]. RSM has been successfully used in various disciplines to optimize, improve, and develop efficient processes to solve challenges that are encountered in time-consuming and inefficient trial-and-error methods [20] [21] [22] [23]. As a result of the unreliable errors often encountered by engineers, scientists, and technologists, manufacturing industries rely greatly on this technique to draw significant conclusions. This method has been reported to predict and correlate the input and output parameters of sliding wear to improve and validate the properties of different engineering materials composites [24] [25] [26]. Dominic et al. [27] developed an empirical relationship to predict the effect of sliding velocity on nano TiB₂ reinforced TiCN cermets and developed the regression equations for wear properties. The mass loss, wear rate and COF were the evaluated responses, and a 95 % confidence level was reported. The sliding velocity significantly affected the responses, and the high R² values confirmed that the model was a good fit for the data. In contrast, the mass loss, wear rate and COF of the composites are demonstrated by residual plots.

TiCN composites are used in operations where high-speed cutting, semi-finishing and high precision are mandatory during application in rigorous environments. However, there is limited research on the wear properties of binderless TiCN-based ceramic reinforced by carbon-based material. To mitigate the challenges imposed by binders in hard materials, we have studied the concept of wear in binderless ceramic

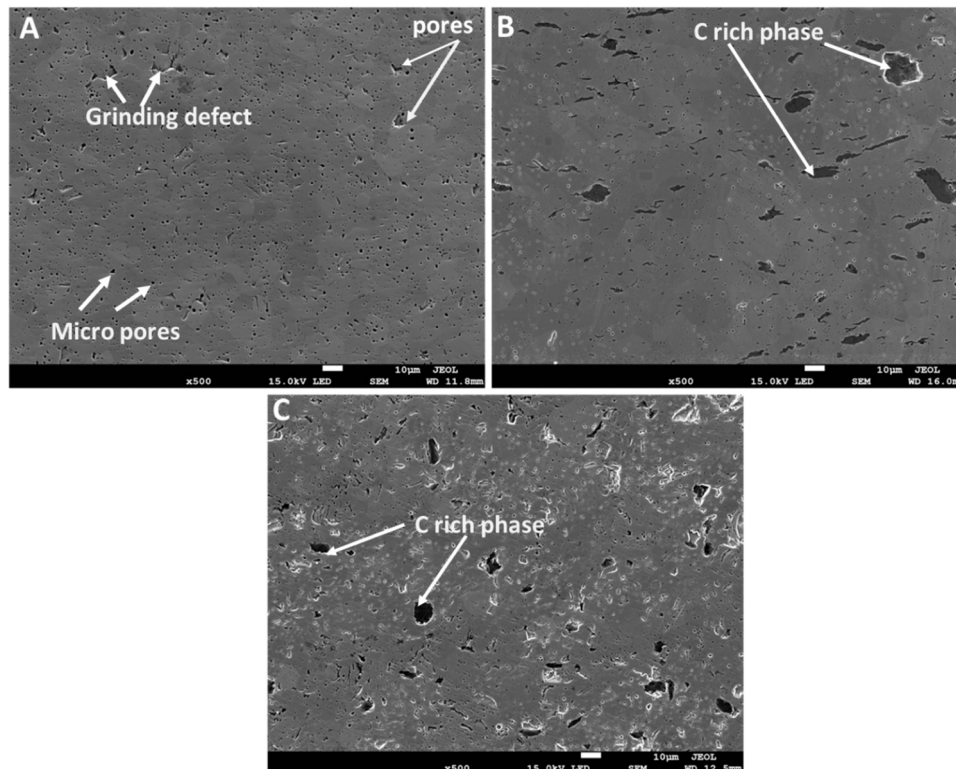


Fig. 1. SEM microstructures of sintered TiC_{0.5}N_{0.5}-Gr ceramic composites: (b) 0 wt%, (b) 0.5 wt% and (c) 1.0 wt% graphite reinforcement.

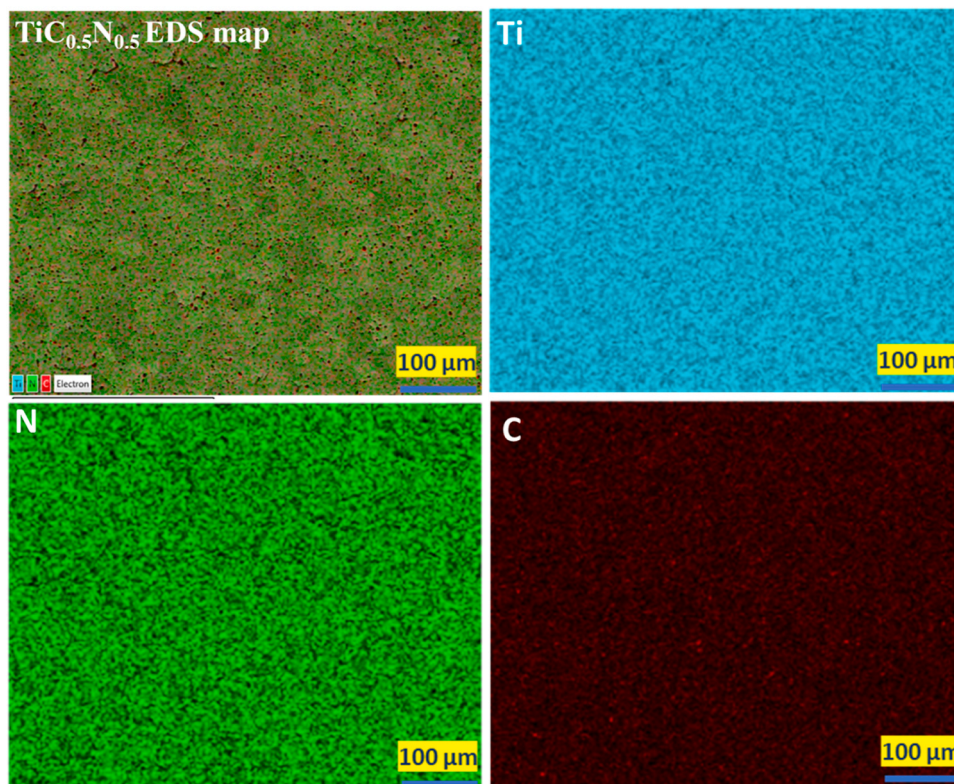


Fig. 2. SEM-EDS mapping of sintered $\text{TiC}_{0.5}\text{N}_{0.5}$ specimen.

composites, emphasising the proportion of reinforcement and applied load for high-speed cutting applications via RSM method and experimental approach. This present study used the UDD approach on RSM to predict the tribological performance of binderless $\text{TiC}_{0.5}\text{N}_{0.5}$ -Gr ceramic composites at ambient temperature. A mathematical model was developed to determine the effect of applied load and graphite reinforcement (input parameters) on wear rate (response variable), and the predicted wear rates are compared against the values obtained from laboratory experiments.

2. Experimental procedure

The sintering procedure and parameters used to fabricate the graphite-reinforced $\text{TiC}_{0.5}\text{N}_{0.5}$ composites have been reported in our previous study [17]. Microstructural characteristics and quantitative analysis of the composition of the sintered $\text{TiC}_{0.5}\text{N}_{0.5}$ -Gr ceramic composites were examined using SEM (FE-SEM JOEL JSM-7900 F) equipped with an energy-dispersive spectroscopy (EDS) detector. In-depth mechanical evaluation of the composites has been reported by Mekgwe et al. [22]; therefore, this study is only focused on evaluating the wear rate of the composites using RSM and laboratory experiments. The composites reinforced with 0, 0.5 and 1.0 wt% of graphite particles are denoted as Sample A, B, and C, respectively.

2.1. Tribology tests

The surfaces of each specimen were prepared by grinding and polishing until a relatively smooth surface was achieved. The $\text{TiC}_{0.5}\text{N}_{0.5}$ -Gr and ruby counterface ball tribo-pairs were thoroughly cleaned and rinsed with acetone to ensure they were free from dirt and grease. The tribology test was performed on a ball-on-disc TRB³, Anton Paar tribometer under dry sliding conditions against a ruby ball ($\text{Al}_2\text{O}_3/\text{Cr}_2\text{O}_3$), with a hardness value of 2300 HV. Table 1 represents the additional test parameters used during the tribology test. Applied loads of 5, 10 and 20

N were used for testing, and the motor speed was maintained at 200 rpm motor speed. Subsequently, the COF variation and wear rate of the composites were estimated and continuously recorded by the tribometer. Post-wear examinations were performed on the worn surface of the specimen using SEM/EDS to evaluate the wear mechanisms.

2.2. Design of experiment: Mathematical modelling by response surface methodology

Design of Experiment (DOE) was used to predict and optimize the wear properties of TiC_xN_y -Gr ceramic composites slid against ruby balls. According to several researchers, this method has proven to be reliable in providing data and merges mathematical and statistical techniques to ascertain the relationship between two or more input factors and their responses [24] [28] [29]. In this study, Design Expert 13 software was used to predict and optimize the wear rate of TiCN -Gr composites. Subsequently, the UDD approach technique was used to develop a mathematical model to determine the effect of graphite reinforcement (0, 0.5 and 1.0 wt%) and applied loads (5, 10, 20 N) on the wear rate of TiCN ceramic composites. The build-up information for the RSM model is represented in Table 2; the factors' coded and actual operating conditions are shown in Table 3.

3. Results and discussion

3.1. Microstructural characteristics of graphite-reinforced $\text{TiC}_{0.5}\text{N}_{0.5}$ ceramic composites

Fig. 1(a-c) shows the SEM micrographs of the sintered graphite reinforced $\text{TiC}_{0.5}\text{N}_{0.5}$ ceramic composites to provide insight into the morphology and distribution of graphite particles on the ceramic hard phase. SEM analysis revealed the distinct microporosity amongst the sintered specimens with 0, 0.5 and 1.0 wt% graphite reinforcement. The effect of graphite on the microstructural characteristics of $\text{TiC}_{0.5}\text{N}_{0.5}$

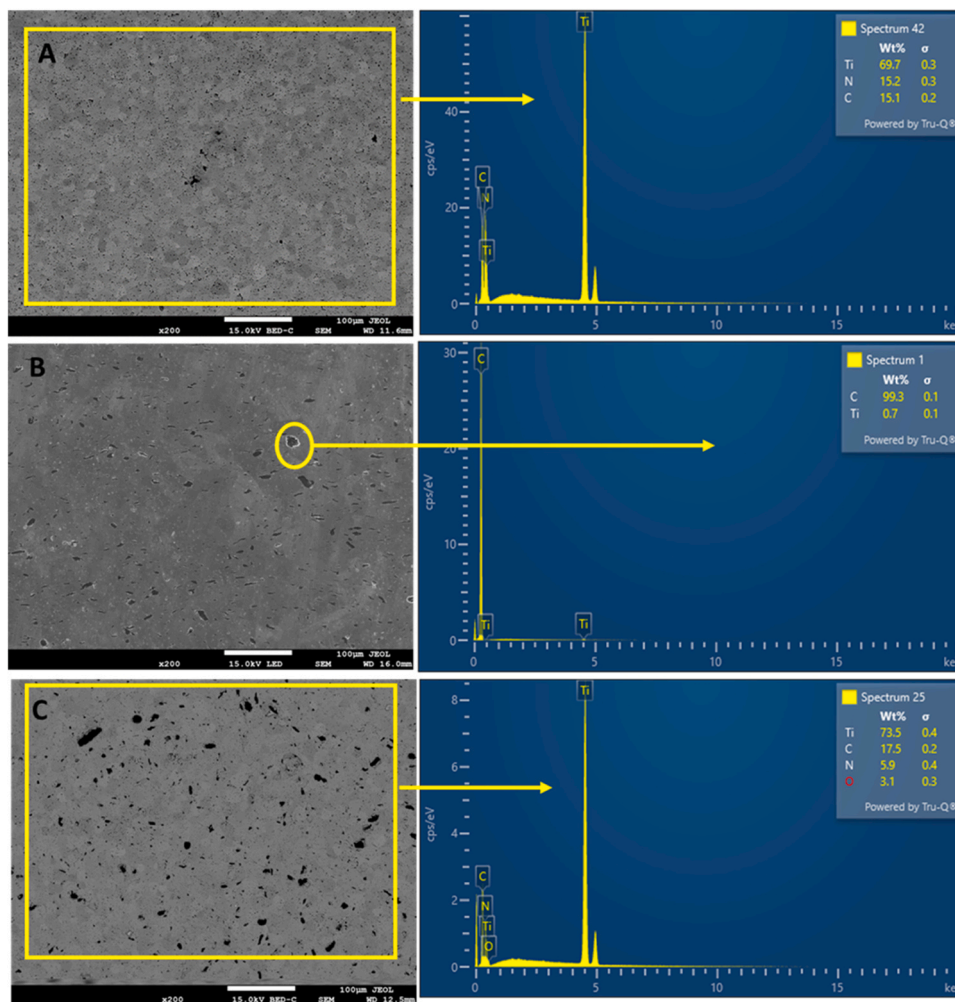


Fig. 3. BSE micrographs of spark plasma sintered TiC_{0.5}N_{0.5}-Gr ceramic composites with EDS spectrum: (a) 0 wt%, (b) 0.5 wt% and (c) 1.0 wt% graphite reinforcement.

ceramic composites was demonstrated, and it can be seen that a proper quantity of graphite reinforcement can be used to achieve a homogenous TiCN microstructure with uniform grains. It was also observed that the micro pores reduce with increased graphite particles. Fig. 1a shows some level of microporosity, which can be ascribed to the failure of proper particle arrangement between TiC and TiN particles during the sintering process. During sintering, reduction reactions occur whereby the gases entrapped become released, which leads to microporosity on the surface of the specimen. Similar observations were reported in previous studies [30] [31]. Furthermore, grinding defects acquired during processing are seen in the specimen, and this can contribute to the porosity observed in the microstructure [17] [32]. Fig. 1b, shows large particles of graphite that are difficult to diffuse into the matrix, as they coalesce to form clusters. In Fig. 1c, the carbon-rich phase is homogeneously distributed on the microstructure. The appearance of the isolated carbon phase in the SEM micrograph suggests the existence of a significant driving force for the segregation of carbon atoms [33] [34] [35]. SEM-EDS analysis was performed to identify the elemental distribution in the sintered specimens, and the EDS mapping of the specimen without graphite is presented in Fig. 2, while a semi-quantitative analysis of the elemental distribution obtained from different positions for the three specimens is shown in Fig. 3. Fig. 2 reveals three distinct phases and confirms the complete homogenization of the TiC and TiN phases into a single-phase TiC_{0.5}N_{0.5} alloy with thermally activated diffusion [16]. Fig. 3(a-c) represents the EDS spectrum used to classify the compositional variations between Ti, C and N phases based on

different proportions of graphite reinforcement. Fig. 3a reveals the composition of the composite with 0 % graphite, 3b denotes 0.5 % graphite, and 3c shows the elemental composition of the specimen with 1 % graphite. Three distinct regions exhibiting variations in composition with respect to shades of grey were observed. A carbon-rich phase characterized the dark spherical region, while light and dark grey areas signify nitrogen and titanium phases, respectively.

3.2. Tribological behavior of TiCN-Gr composites

To understand the effect of graphite addition and applied load on the tribological properties of binderless TiCN ceramic composites, the wear behaviour of the specimens against ruby ball counterface was evaluated. The binderless TiCN ceramic composites are considered promising cutting tool inserts due to lower COF and excellent wear resistance, which is suitable for application in severe environments.

3.2.1. Wear rate

The wear rate used to assess the behaviour of TiCN-Gr composites is represented in Fig. 4. Comparing the behaviour of the composites under different loads and graphite addition, the wear rate significantly decreased as the graphite content increased. During sliding wear tests, tribo-pair is exposed to friction when in contact at relative motion. During sliding wear tests, the tribo-pair is subjected to friction when the asperity contacts are sheared, and friction is generally regarded as the main cause of wear and energy loss of the sliding system [36]. From the

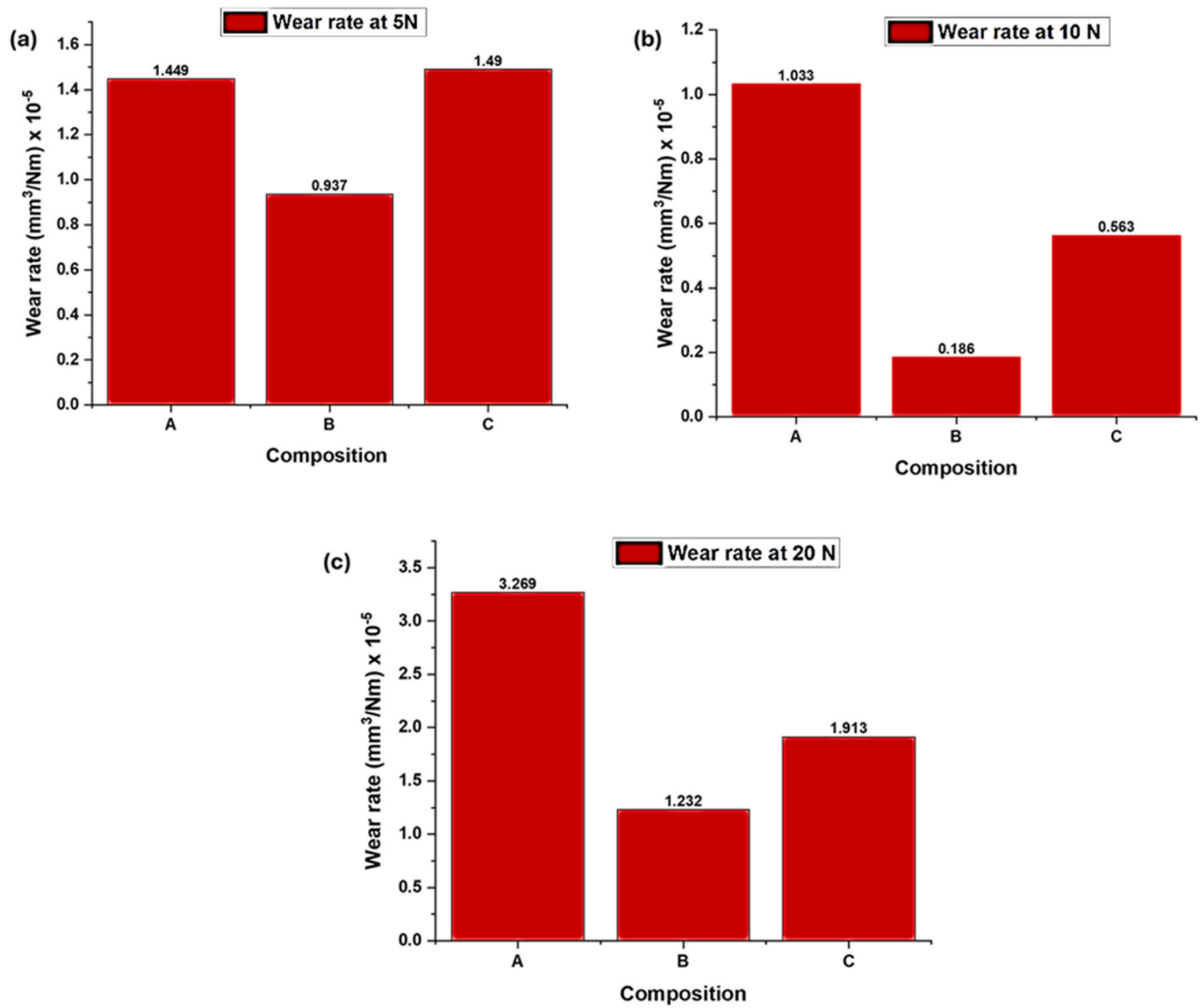


Fig. 4. The wear rate of $\text{TiC}_{0.5}\text{N}_{0.5}\text{-Gr}$ composites: (a) 5 N, (b) 10 N and (c) 20 N.

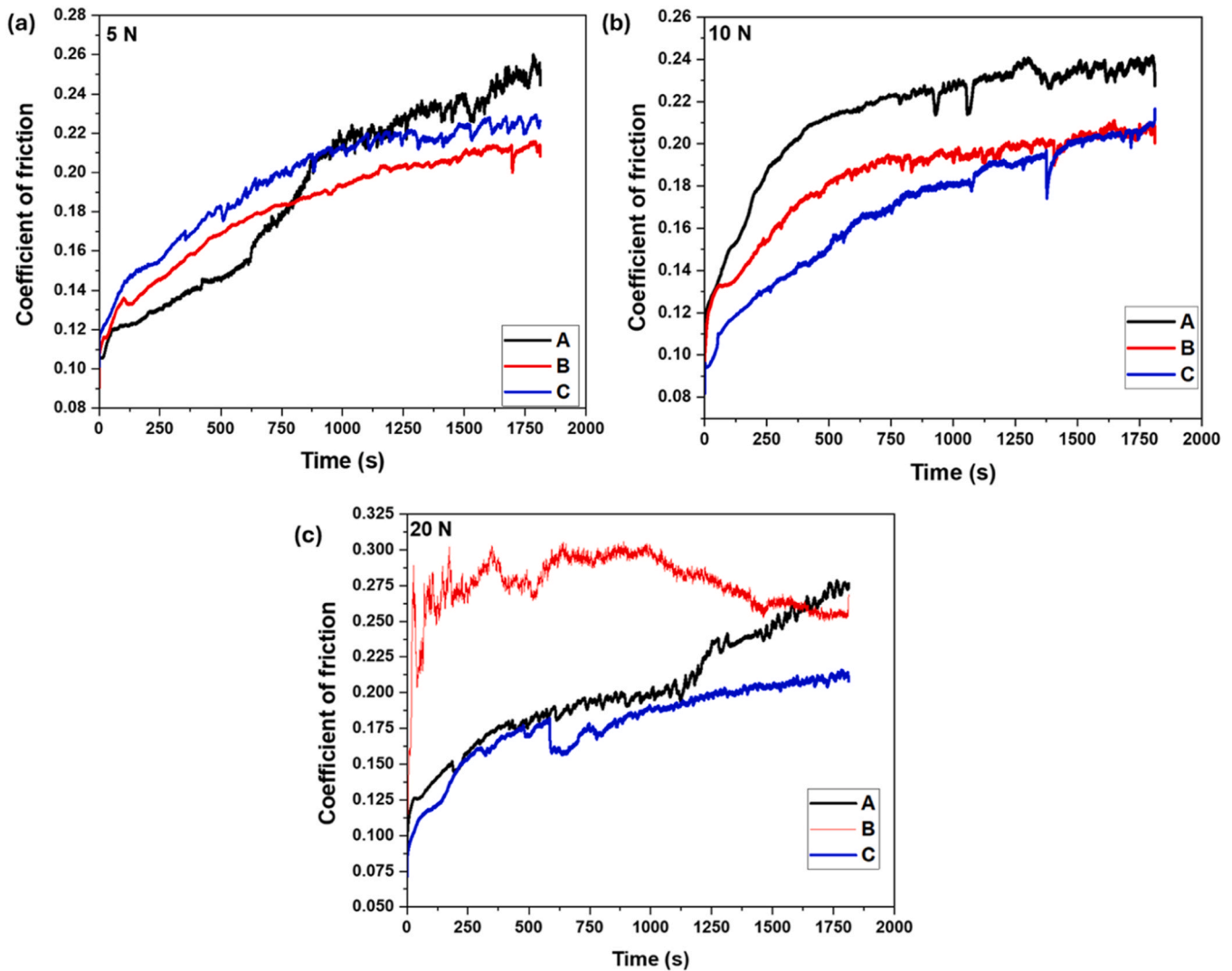


Fig. 5. Coefficient of friction against time for $\text{TiC}_{0.5}\text{N}_{0.5}\text{-Gr}$ composites against ruby ball: (a) 5 N, (b) 10 and (c) 20 N loads.

wear rate results (Fig. 4), it can be seen that the wear rate of the composites without graphite addition was higher than that of the composites with graphite content. The literature on the wear properties of TiCN-based cermets has shown poor wear resistance, and the wear rate varies on the order of 10^{-6} to 10^{-7} [37] [4] However, the wear resistance of the composites was significantly enhanced with 0.5 wt% addition of graphite and lower wear rate values of 0.937×10^{-5} , 0.186×10^{-5} , and 1.232×10^{-5} were recorded at 5 N, 10 N, and 20 N applied loads, respectively.

Notably, the wear test conducted on TiCN-Gr using a load of 20 N exhibited improved wear resistance than those performed using 5 N and 10 N. In general, the wear rate increases with an increase in applied load, and as the load was increased to 20 N, the wear rate increased irrespective of the composition. This increase can be attributed to the increased mechanical stresses and frictional heat subjected to the working interface. The decreased wear rate at 0.5 wt% graphite reinforcement could be attributed to the lubricating effect of graphite. During sliding, an adequate amount of graphite provides a tribo-film on the surface of the material which enhances its tribological properties. When graphite is introduced as a solid lubricant on the TiCN matrix, the extruded graphite particles form a lubricant tribo-film and protects the surface of the composites from the hard abrasive particles [38]. However, according to the microstructures reported in Fig. 1c, the homogeneous distribution of graphite particles within the TiCN matrix

prevented the extrusion of its particles and provided solid lubricating properties.

3.2.2. Coefficient of friction

The coefficient of friction measured from the recorded frictional force and the applied pressure on the surface of the specimen is shown in Fig. 5. The average COF values for this study were in the range of 0.164 – 0.276, which is lower when compared to the TiCN material with and without binder addition [39] [40], the COF values varied from 0.46 - 0.75 at 20 - 50 N respectively [41] [42]. During wear tests, there is a slight frictional temperature rise, which causes the decomposition of graphite particles from the matrix [43]. It further migrates to the surface of the specimen and reacts with titanium, thereby forming a tribo-layer at the contact surface during sliding.

From the COF variation plots represented in Fig. 5a, the variations of COF at 5 N show that the composition without graphite exhibits the highest COF values as compared to other compositions, and a similar observation is seen at a load of 10 N (Fig. 5b). The decrease in the COF of graphite-reinforced $\text{TiC}_{0.5}\text{N}_{0.5}$ can be attributed to the solid lubricating properties imparted by graphite to enhance the tribological properties of the ceramic composite. A similar observation was reported in a previous study [44]. In contrast, at a load of 20 N, there is little or no formation of tribo-film at the composite surface with 0.5 wt% graphite. This might result from the higher frictional force generated between the specimen

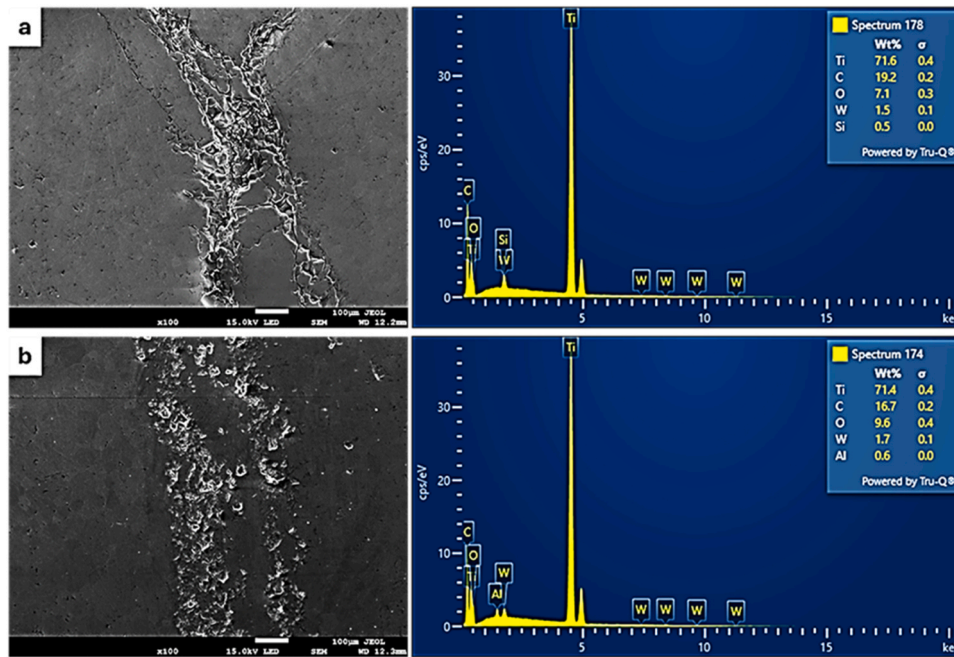


Fig. 6. SEM micrographs of the worn surface of $\text{TiC}_{0.5}\text{N}_{0.5}\text{-Gr}$ composite (a) specimen A at 5 N and (b) specimen B at 20 N and the corresponding EDS spectrum.

Table 4

The actual design factors and the response.

Run	Factor 1 Graphite (wt%)	Factor 2 Load (N)	Response Wear rate (mm^3/Nm)
1	1	10	5.63E-06
2	0	20	3.27E-05
3	1	20	1.913E-05
4	0.5	20	1.23E-05
5	0	5	1.45E-05
6	0	10	1.03E-05
7	0.5	5	9.37E-06
8	1	5	1.49E-05
9	0.5	10	1.864E-06

Where: A represents the coded value for graphite content and B represents the coded value for applied load.

and counterface material due to the increased load, which decreased its COF [1]. According to Fig. 5c, the specimen reinforced with 1 wt% graphite exhibits the lowest COF value of 0.178 compared to 0.202 and 0.276, respectively, recorded by 0 % and 0.5 % reinforced specimens, and this can be attributed to the ease of tribo-film formation owing to the free graphite, which acts as a solid lubricant that promotes the formation of oxide layer on the surface of the specimen during the test [39].

3.2.3. Surface morphology of worn $\text{TiC}_{0.5}\text{N}_{0.5}\text{-Gr}$ composites

The worn surface is analysed to understand the dominating wear mechanisms under sliding conditions. The known wear mechanisms for TiCN material include abrasion, adhesion, surface fatigue, fracture, and grain pull-out [45] [44]. Fig. 6a shows the SEM micrographs of the worn surfaces of the TiCN-Gr composites. The worn surface of the specimen with 0.5 wt% graphite depicts adhesive wear due to evident surface particle removal in the microstructure. The EDS analysis further confirms the formation of oxide layers owing to the heat generated between the two sliding surfaces [40]. Oxidative wear is the primary mechanism evident in Fig. 6b, as the microstructure shows a slight pulling of the surface layer of the specimen by the counterface ball due to the formation of small lubrication between the sliding surfaces at higher load (20 N). Notably, the metal surface becomes oxidized by air, which can result in the peeling of the metal oxide film under continuous friction

[12]. Based on these findings, it can be concluded that binderless TiCN composites display enhanced wear resistance compared to TiCN-based cermets, and adequate graphite content can provide the required lubrication for the composites to improve the wear resistance against ruby balls further. The presence of graphite reinforcement within the TiCN matrix could provide a strong bond between the reinforcement and the matrix phase due to mechanical interlocking, chemical bonding, or both, thus ensuring effective load transfer from the matrix to the reinforcement. It is also noteworthy that the matrix distributes the load among the reinforcement particles, and this often increases the resistance of the TiCN composite to the applied load. Moreover, the frictional behaviour of the composite is enhanced due to the lubricating effect of the graphite particles during the wear test. This is evident in Figs. 6a and 6b, as increased load does not rapidly deteriorate the surface of the specimens.

4. Design of experiment results

4.1. Numerical modelling

The empirical relationship to predict the wear rate of $\text{TiC}_{0.5}\text{N}_{0.5}\text{-Gr}$ composites was recognized as the applied load and the graphite content, and the experimental results were analyzed through RSM to obtain the empirical model. The second-order polynomial regression in Eq. 1 was used for the designated input parameters to signify the response surface “Y”.

$$= \beta_0 + \sum_{j=1}^k \beta_j X_j + \sum_{j=1}^k \beta_{jj} X_j^2 + \beta_0 + \sum_{i=1}^k \sum_{<j=2}^k \beta_{ij} X_i X_j + e_i \quad (1)$$

Where:

Y is the predicted response, k is the number of studied factors, X_i and X_j are the variables (factors), β_0 is the constant coefficient, β_j , β_{jj} , β_{ij} are the interaction coefficients of linear, quadratic, and second-order terms, and e_i is the error.

A total number of 9 experimental runs were given (Table 4) and all the coefficients were tested for their significance at 95 % confidence using a Design expert statistical software package. After determining the significant coefficients, the final models were developed using only these coefficients and the final mathematical models were developed to

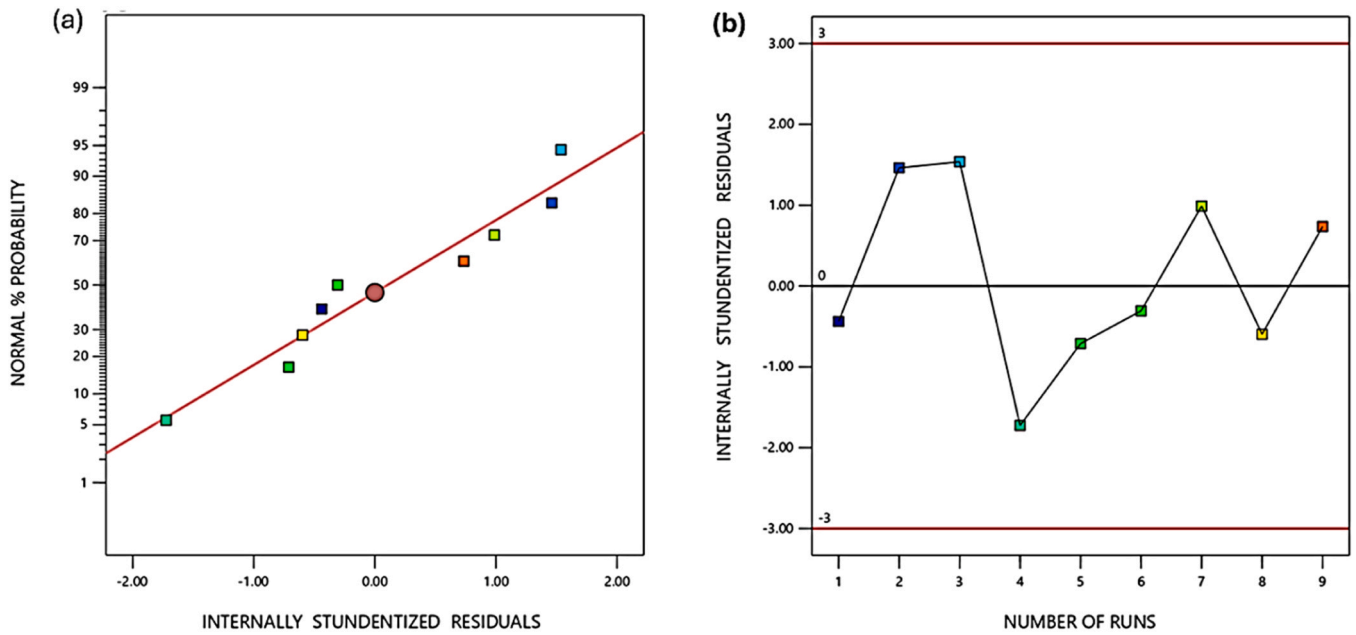


Fig. 7. Residual plots: (a) Normal plot of residual and (b) residuals vs runs.

Table 5

ANOVA results of the suggested quadratic model.

Source	Sum of squares	Degree of freedom	Mean square	F-value	P-value	
Model	0.0000	5	2.345E-06	24.63	0.0122	Significant
A-A	9.017E-07	1	9.017E-07	9.47	0.0542	
B-B	1.373E-06	1	1.373E-06	14.43	0.0320	
AB	4.423E-07	1	4.423E-07	4.65	0.1201	
A ²	3.104E-06	1	3.104E-06	32.62	0.0106	
B ²	4.811E-06	1	4.811E-06	50.55	0.0057	
Residual	2.855E-07	3	9.517E-08			
Cor Total	0.0000	8				

Standard deviation: 0.0003, R^2 : 0.9762, adjusted R^2 : 0.9366 and predicted R^2 : 0.7412.

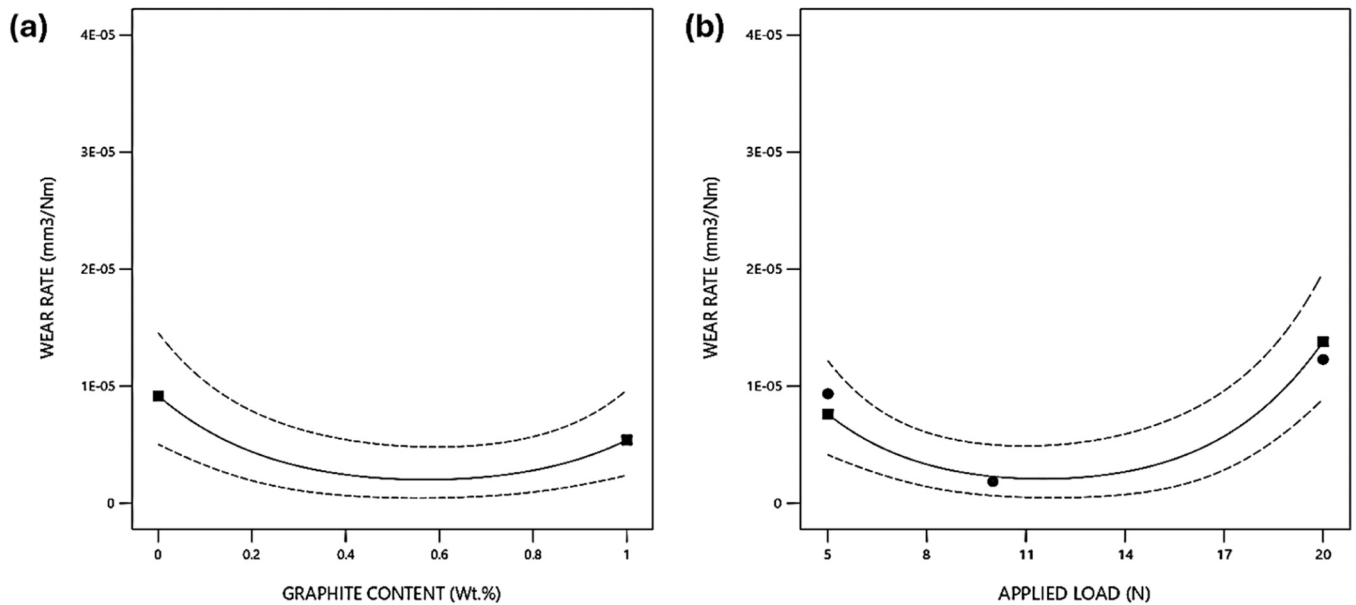


Fig. 8. One factor interaction of the variable on the wear rate.

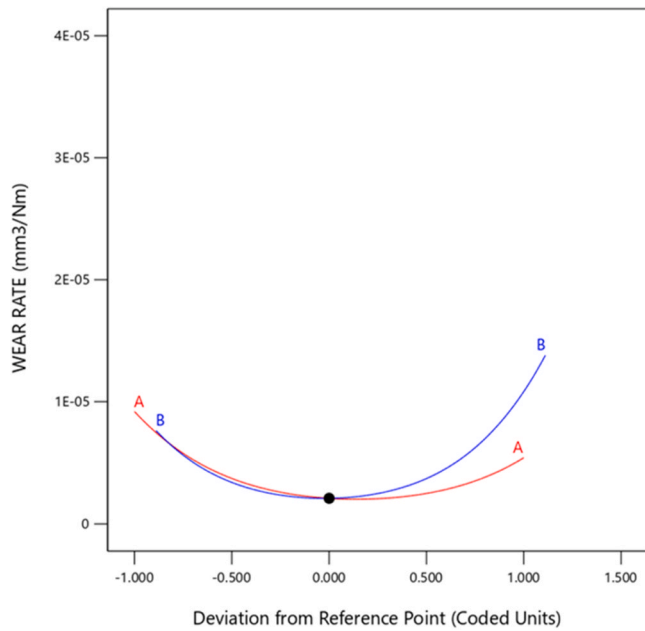


Fig. 9. Perturbation plot for wear rate.

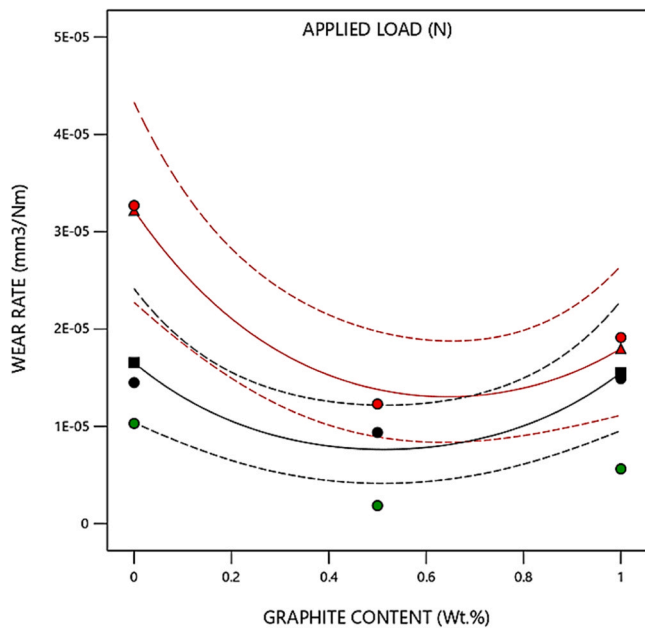


Fig. 10. Interactions of the variables on the wear rate.

estimate the wear rate. For this study, the independent variables were coded as A and B, and the mathematical expression for the wear rate with A and B variables is shown in Eq. 2.

$$(R1) = + 0.0014 - 0.0004*A + 0.0005*B - 0.0003*AB + 0.0012*A^2 + 0.0018*B^2 \quad (2)$$

4.2. Residual analysis

Residual is the distinction of the responses between the experimental and the predicted and is significantly used to ascertain the model adequacy. Fig. 7 represents the residual analysis employed to validate the hypothesis that they are independent of each other [46]. It is recognized that the positive value of residual illustrates low prediction while the

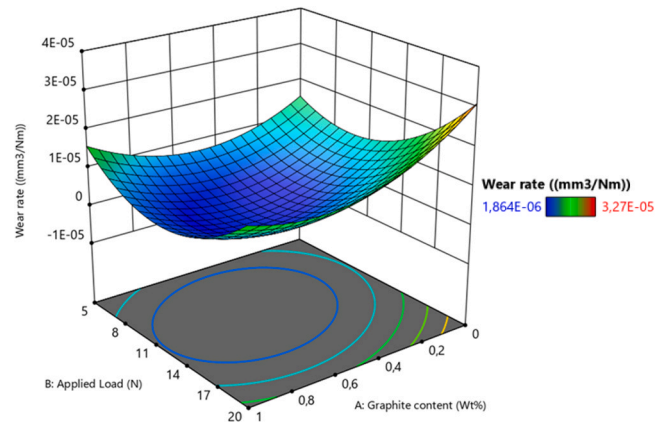


Fig. 11. 3D surface plots between graphite content and load on the wear rate.

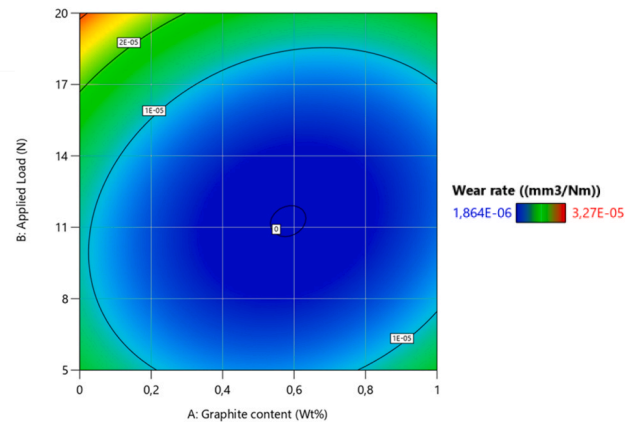


Fig. 12. 2D surface plot of interaction between applied load and graphite content on the wear rate.

negative value represents high predictions. The invalidity of the normality assumption is denoted by the dissemination of points along the straight line, and if the points are diverged from the straight line, then the normality assumptions are invalid. Fig. 7a shows the normal probability plot of the residuals for wear rate drawn to evaluate the normality of the data. It can be seen that the residuals fall along the straight line, indicating that the error is normally distributed and that the assumptions are valid. Fig. 7b shows residual vs number of runs and the internally studentized residuals suggested by the model were used. This plot is used to verify the hypothesis that the residuals are independent of each other. It can be seen that there are no decreasing or increasing patterns in the points obtained because all the run residual lies on or amongst the levels of - 3 to 3.

4.3. Analysis of variance (ANOVA)

The ANOVA technique recommends whether the proposed regression model for optimising process variables is adequate and significant; the correlation coefficient (R^2) reveals the proper fit for the model. The value of correlation (R^2) for the regression model is 0.9762, which demonstrates that 97.62 % of the experimental data fits into the developed model and the predicted R^2 of 0.7412 is in good agreement with the adjusted R^2 of 0.9366 [47] [48]. The model F-value and P-value are used to verify the significance of the model. A P-value less than 0.0500 indicates that the model terms (B , A^2 , and B^2) are significant, while values greater than 0.1000 show they are insignificant. The coded factors equation can be used to predict the response for given levels of each factor. By default, the high levels of the factors are coded as + 1, and the low levels are coded as - 1. The coded equation is useful for

Table 6
Coefficients in terms of the coded factors for the wear rate.

Factor	Coefficient Estimate	Degree of freedom	Standard Error	95 % CI Low	95 % CI High	VIF
Intercept	0.0014	1	0.0003	0.0006	0.0023	
A-A	-0.0004	1	0.0001	-0.0008	0.0000	1.02
B-B	0.0005	1	0.0001	0.0001	0.0009	1.04
AB	-0.0003	1	0.0002	-0.0008	0.0002	1.02
A ²	0.0012	1	0.0002	0.0006	0.0019	1.0000
B ²	0.0018	1	0.0002	0.0010	0.0026	1.04

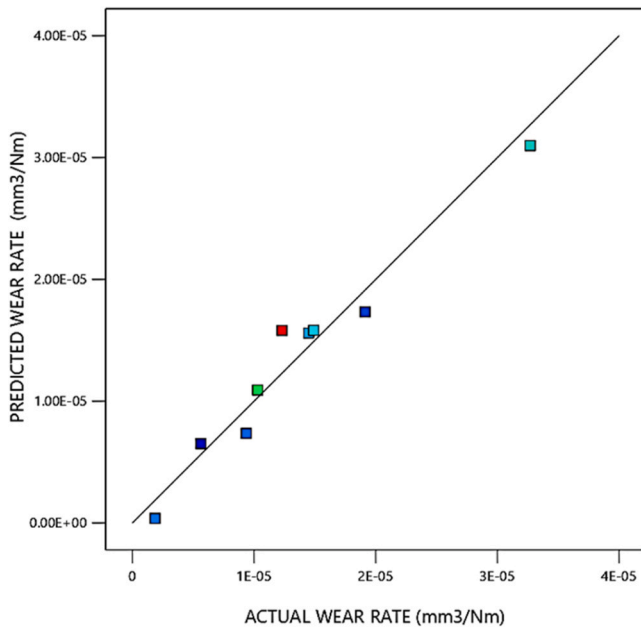


Fig. 13. Predicted vs actual plots for wear rate.

identifying the relative impact of the factors by comparing the factor coefficients [25]. Based on the results observed in Table 5, the model F-value is 24.63, whereas the P-value of 0.0122 is less than 0.05, which indicates that the model is significant, making B, A², B² significant model terms. Fig. 8 shows the distinct behaviour of the two factors used to determine the wear resistance of TiC_{0.5}N_{0.5}-Gr composites. Fig. 8a and b represent the relationship between graphite content and applied load as a function of the wear rate, respectively. In Fig. 8a, the wear rate is seen to decrease with increased graphite content, whereas the wear rate first decreases up to 10 N in Fig. 8b but increases as the load rises to 20 N. This behaviour agrees with the experimental results, which recorded a noticeable decrease in the wear rate of specimen reinforced

with 0.5 wt% graphite content when a load of 10 N was applied.

4.3.1. ANOVA analysis for model validation

ANOVA analysis was performed to summarize and develop the data for the wear test results, including perturbation plot, interaction effect, prediction vs. actual result, and a 3D response surface. These graphs are used to look at the impact of applied load and graphite content on the wear rate behaviour of TiCN ceramic composites.

4.3.2. Perturbation plot

The perturbation plot illustrates the effect of all the factors at optimal experimental conditions and also assists in evaluating the impact of all factors at a focal point in the design. This is represented by the sharpness of the curve, where the factors tend to be significant in the response [49]. A perturbation plot to assess the effect of all the process parameters at the midpoint on the wear rate is displayed in Fig. 9. It can be observed with an increase of applied load from a low level (−1) to a high level (+1), the wear rate of TiC_{0.5}N_{0.5}-Gr composite increases. It has been reported that the load is one of the critical parameters influencing the wear rate of the material [24]. As the content of graphite reinforcement increased, the wear rate decreased, which can be attributed to the solid lubricating properties of graphite [13].

4.3.3. Optimization and interaction effect of variables on wear rate.

RSM was used to optimize variables that appreciably affect the wear rate of the TiCN composites. The optimization of the reinforcement addition is crucial to ensure the composite meets the desired micro-structural and mechanical properties of the final application for the composite being fabricated. Fig. 10 represents the interactions of the two variables (applied load and wt% of graphite) on the response (wear rate) to determine the potential relationship. It can be established that an increase in graphite reinforcement and decreased load will result in a reduced wear rate. However, 0.5 wt% of graphite at an applied load of 10 N exhibits enhanced wear resistance of TiC_{0.5}N_{0.5}-Gr composites against the ruby ball counterface. The two independent variables are plotted on the X and Y axis, and the relationship is illustrated by the 3D and 2D contour plots as illustrated in Figs. 11 and 12, respectively. The effect of these input variables can be noticeably identified in both contour plots by different colours in Fig. 11. The blue colour in Fig. 12 represents the minimum value, the green depicts the average value, and the red signifies the maximum value. From these plots, the wear rate is maximum when the graphite content is 0 wt% under an applied load of 20 N. According to the plots, the 0.5 wt% graphite addition exhibited the optimal experimental condition, with an enhanced wear resistance at an applied load of 10 N, but optimal interactions are observed between 0.4 – 0.8 wt% graphite reinforcement and 8 – 14 N applied loads.

4.3.4. Validation of the model

From this study, the difference between the predicted R² (0.9366) and the adjusted R² (0.7412) is 0.1954, which is less than 0.2; therefore, the model can be considered as valid. The Adeq precision, which measures the signal to ratio, records a ratio value of 16.598 for the wear rate. This is acceptable; hence, the model can be used for analysis in the design space. Table 6 represents the coefficients in terms of the coded factors and the predictability of the wear model, which is at a confidence

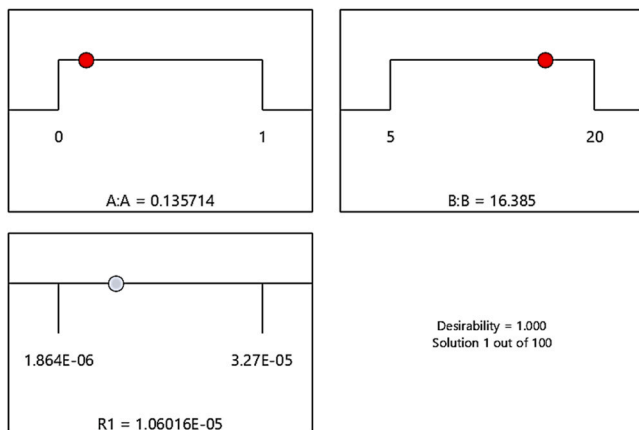


Fig. 14. Optimization results for wear rate.

Table 7
Report on the wear rate model.

Run Order	Actual Value	Predicted Value	Residual	Leverage	Internally Studentized Residuals	Externally Studentized Residuals	Cook's Distance	Influence on Fitted Value DFFITS	Standard Order
1	0.0024	0.0024	-0.0001	0.567	-0.375	-0.313	0.031	-0.359	6
2	0.0057	0.0057	0.0001	0.853	0.443	0.374	0.190	0.902	7
3	0.0044	0.0042	0.0001	0.853	1.210	1.381	1.418 ⁽¹⁾	3.328 ⁽¹⁾	9
4	0.0035	0.0037	-0.0002	0.556	-0.950	-0.928	0.188	-1.037	8
5	0.0038	0.0041	-0.0002	0.746	-1.597	-3.373	1.249 ⁽¹⁾	-5.780 ⁽¹⁾	1
6	0.0032	0.0030	0.0002	0.567	0.966	0.950	0.204	1.088	4
7	0.0031	0.0027	0.0003	0.556	1.533	2.690	0.490	3.007 ⁽¹⁾	2
8	0.0039	0.0039	-0.0001	0.746	-0.431	-0.363	0.091	-0.622	3
9	0.0014	0.0015	-0.0001	0.556	-0.583	-0.506	0.071	-0.565	5

⁽¹⁾ Exceeds limits.

level of 95 %. Fig. 13 demonstrates a linear plot, which compares the actual and the predicted response obtained for the wear rate. The accuracy of the model is evident from the linear line seen in the plot, and the predicted values correspond with the measured data obtained from the laboratory experiments. Optimization studies were further performed to determine the possible factors that can be responsible for achieving minimum wear rate for enhanced wear resistance of the TiC_{0.5}N_{0.5} composites. From the results, the desirability of 1.00 and one solution was achieved for the optimum level of factors and performance (Fig. 14). The report of the wear rate model is presented in Table 7.

5. Conclusion

In this study, a mathematical model was adopted to predict the wear properties of graphite-reinforced binderless TiC_{0.5}N_{0.5} in dry sliding wear conditions against a ruby ball. The following are deduced from this investigation:

- RSM (UDD approach) technique was effectively used to develop a mathematical model to determine the effect of graphite content and applied load on the wear rate.
- There was good agreement between the experimental and the predicted value by RSM, P-value of 0.0122, R² = 0.9762 % and 95 % confidence level was achieved. And this clearly indicates that the model is significant and acceptable.
- The 3D surface and contour plots in response surface methodology indicated that the graphite content greatly influenced the wear rate. As graphite reinforcement increased, minimal wear rate was noticeable and optimal interaction between 0.4 and 0.8 wt% graphite was observed at 8 – 14 N applied load.
- Tribo-film formation was not present on the surface of a composite with 0.5 wt% graphite content is owing to the higher friction and higher applied load, which increases the COF.
- Binderless TiC_{0.5}N_{0.5} showed enhanced wear resistance against ruby ball, and the dominating wear mechanisms were identified as abrasion, adhesion and oxidative.

CRedit authorship contribution statement

Peter Apata Olubambi: Writing – review & editing, Supervision, Data curation, Conceptualization. **Ojo Jeremiah Akinribide:** Writing – original draft, Supervision, Conceptualization. **Samuel Akinwamide:** Writing – review & editing, Supervision, Conceptualization. **Elvis Mdu**

Gonya: Writing – review & editing, Software, Funding acquisition. **Gadifele Nicolene Mekgwe:** Writing – original draft, Methodology, Formal analysis, Data curation, Conceptualization. **Emmanuel Olorundaisi:** Validation, Methodology, Formal analysis, Data curation.

Declaration of Competing Interest

The authors declare that they have no known competing financial interests or personal relationships that could have appeared to influence the work reported in this paper.

Data availability

Data will be made available on request.

Acknowledgment

The authors are grateful to National Research Foundation of South Africa, for providing the funding used for this research.

References

- [1] Grigoriev ON, et al. Wear-Resistant TiCN-Based Ceramic Materials for High-Load Friction Units. Powder Metall Met Ceram 2021;vol. 59(9–10):528–36. <https://doi.org/10.1007/s11106-021-00194-5>.
- [2] Akinribide OJ, Mekgwe GN, Obadele BA, Ajibola OO, Akinwamide SO, Olubambi PA. Microstructural and phase evolution of spark plasma sintering of graphitized Ti (C<inf>0.9</inf>N<inf>0.1</inf>) composites. Int J Refract Met Hard Mater 2019;vol. 78. <https://doi.org/10.1016/j.ijrmhm.2018.09.013>.
- [3] Akinribide OJ, Mekgwe GN, Ajibola OO, Obadele BA, Akinwamide SO, Olubambi PA. Studies on Mechanical properties of graphite reinforced Ti (Cx, N1-x) using nanoindentation techniques. Procedia Manuf 2019. <https://doi.org/10.1016/j.promfg.2019.02.085>.
- [4] Peng Y, Miao H, Peng Z. Development of TiCN-based cermets: mechanical properties and wear mechanism. Int J Refract Met Hard Mater 2013;vol. 39:78–89. <https://doi.org/10.1016/j.ijrmhm.2012.07.001>.
- [5] Shankar E, Prabu SB, Padmanabhan KA. Mechanical properties and microstructures of TiCN/nano-TiB₂/TiN cermets prepared by spark plasma sintering. Ceram Int 2018;vol. 44(8):9384–94. <https://doi.org/10.1016/j.ceramint.2018.02.154>.
- [6] Xiong H, Wen Y, Gan X, Li Z, Chai L. Influence of coarse TiCN content on the morphology and mechanical properties of ultrafine TiCN-based cermets. Mater Sci Eng: A 2017;vol. 682:648–55. <https://doi.org/10.1016/j.msea.2016.11.085>.
- [7] Verma V, Manoj Kumar BV. Processing of TiCN–WC–Ni/Co cermets via conventional and spark plasma sintering technique. Trans Indian Inst Met 2017; vol. 70(3):843–53. <https://doi.org/10.1007/s12666-017-1069-y>.
- [8] Ragothuman A, Kanthi Natarajan GV, Shanmugavel BP. Wear and thermal stability of TiCN–WC–Co–Cr₃C₂ cermets modified by TiN. Int J Refract Met Hard Mater 2019;vol. 84:105020. <https://doi.org/10.1016/j.ijrmhm.2019.105020>.

- [9] Gao J, Song J, Lv M, Cao L, Xie J. Microstructure and mechanical properties of TiC_{0.7}N_{0.3}-HfC cermet tool materials. *Ceram Int* 2018;vol. 44(15):17895–904. <https://doi.org/10.1016/j.ceramint.2018.06.262>.
- [10] Veerapanaicker Soundaraj P, Sembulingam SS, Shanmugavel BP. On the role of B4C on hardness and toughness of TiCN - SiC - TiN - Cr3C2 - Co cermet. *Int J Refract Met Hard Mater* 2020;vol. 90:105252. <https://doi.org/10.1016/j.jmrhm.2020.105252>.
- [11] Sembulingam SS, Soundaraj PV, Shanmugavel BP. Enhanced thermal stability and wear resistance of TiCN-SiC-TiN-Cr3C2-Co cermet modified by B4C for cutting tool application. *Int J Refract Met Hard Mater* 2020;vol. 93:105352. <https://doi.org/10.1016/j.jmrhm.2020.105352>.
- [12] Zhou L, Xiong J, Guo Z, Ye J. Design and preparation of gradient graphite/cermets self-lubricating composites. *J Mater Sci Technol* 2018;vol. 34(8):1378–86. <https://doi.org/10.1016/j.jmst.2017.09.018>.
- [13] Wang H. Graphite Solid Lubrication Materials. in *Encyclopedia of Tribology*. Boston, MA: Springer US; 2013. p. 1550–5. https://doi.org/10.1007/978-0-387-92897-5_1261.
- [14] Chand Yadav P, Kumar Sharma S, Venkata Manoj Kumar B, Kang S. Effect of linear velocity on sliding wear behavior of TiCN based cermets. *Mater Today Proc* 2018; vol. 5(9):17342–9. <https://doi.org/10.1016/j.matpr.2018.04.147>.
- [15] Stewart TL, Plucknett KP. The sliding wear of TiC and Ti(C,N) cermets prepared with a stoichiometric Ni3Al binder. *Wear* 2014;vol. 318(1–2):153–67. <https://doi.org/10.1016/j.wear.2014.06.025>.
- [16] Akinribide OJ, et al. Sintering of binderless TiN and TiCN-based cermet for toughness applications: Processing techniques and mechanical properties: a review. *Ceram Int* 2019;vol. 45(17):21077–90. <https://doi.org/10.1016/j.ceramint.2019.07.191>.
- [17] Mekgwe GN, Akinribide OJ, Akinwamide SO, Olubambi PA. Fabrication of graphite reinforced TiCxNy by spark plasma sintering technique: A comparative assessment of microstructural integrity and nanoindentation properties. *Vacuum* 2021;vol. 187:110144. <https://doi.org/10.1016/j.vacuum.2021.110144>.
- [18] Mekgwe GN, Akinribide OJ, Langa T, Obadele BA, Olubambi PA, Lethabane LM. Effect of graphite addition on the tribological properties of pure titanium carbonitride prepared by spark plasma sintering. *IOP Conf Ser: Mater Sci Eng* 2019. <https://doi.org/10.1088/1757-899X/499/1/012011>.
- [19] Lamidi S, Olaleye N, Bankole Y, Obalola A, Aribike E, Adigun I. Applications of Response Surface Methodology (RSM) in Product Design, Development, and Process Optimization. in *Response Surface Methodology - Research Advances and Applications*. IntechOpen,; 2023. <https://doi.org/10.5772/intechopen.106763>.
- [20] Roush WB, Petersen RG, Arscott GH. An application of response surface methodology to research in poultry nutrition. *Poult Sci* 1979;vol. 58(6):1504–13. <https://doi.org/10.3382/ps.0581504>.
- [21] Santos Mendonça RC, Morelli AMF, Pereira JAM, de Carvalho MM, de Souza NL. Prediction of Escherichia coli O157:H7 adhesion and potential to form biofilm under experimental conditions. *Food Control* 2012;vol. 23(2):389–96. <https://doi.org/10.1016/j.foodcont.2011.08.004>.
- [22] Chi G, Hu S, Yang Y, Chen T. Response surface methodology with prediction uncertainty: A multi-objective optimisation approach. *Chem Eng Res Des* 2012;vol. 90(9):1235–44. <https://doi.org/10.1016/j.cherd.2011.12.012>.
- [23] Donis-González IR, Guyer DE, Pease A. Application of Response Surface Methodology to systematically optimize image quality in computer tomography: A case study using fresh chestnuts (*Castanea spp.*). *Comput Electron Agric* 2012;vol. 87:94–107. <https://doi.org/10.1016/j.compag.2012.04.006>.
- [24] Selvi S, Rajasekar E. Theoretical and experimental investigation of wear characteristics of aluminum based metal matrix composites using RSM. *J Mech Sci Technol* 2015;vol. 29(2):785–92. <https://doi.org/10.1007/s12206-015-0140-z>.
- [25] Kumar R, et al. Effect of particle size and weight fraction of SiC on the mechanical, tribological, morphological, and structural properties of Al-5.6Zn-2.2Mg-1.3Cu composites using RSM: fabrication, characterization, and modelling. *Heliyon* 2022; vol. 8(9):e10602. <https://doi.org/10.1016/j.heliyon.2022.e10602>.
- [26] Vettivel SC, Selvakumar N, Narayanasamy R, Leema N. Numerical modelling, prediction of Cu-W nano powder composite in dry sliding wear condition using response surface methodology. *Mater Des* 2013;vol. 50:977–96. <https://doi.org/10.1016/j.matdes.2013.03.072>.
- [27] Dominic Merwin Xavier AM, Neevatha SB, Swathi Selvi S, Shanmugavel BP, Padmanabhan KA. Wear and thermal stability of nano-TiB₂ modified TiCN-WC-Co-Cr₃C₂ cermet. *Int J Refract Met Hard Mater* 2020;vol. 86:105130. <https://doi.org/10.1016/j.jmrhm.2019.105130>.
- [28] Yolmeh M, Jafari SM. Applications of Response Surface Methodology in the Food Industry Processes. *Food Bioproc Tech* 2017;vol. 10(3):413–33. <https://doi.org/10.1007/s11947-016-1855-2>.
- [29] Banerjee S, Sutradhar G. “Study on Wear Behaviour of Mg-Gr-WC Nanocomposite Using Response Surface Methodology,” Part 3 *Mater Today Proc* 2018;vol. 5(9): 17664–73. <https://doi.org/10.1016/j.matpr.2018.06.086>.
- [30] Lengauer W, Scagnetto F. Ti(C,N)-Based Cermets: Critical Review of Achievements and Recent Developments. *Solid State Phenom* 2018;vol. 274:53–100. <https://doi.org/10.4028/www.scientific.net/SSP.274.53>.
- [31] Zhao Y, Zheng Y, Zhou W, Zhang J, Huang Q, Xiong W. Effect of carbon addition on the densification behavior, microstructure evolution and mechanical properties of Ti(C, N)-based cermets. *Ceram Int* 2016;vol. 42(4):5487–96. <https://doi.org/10.1016/j.ceramint.2015.12.097>.
- [32] Wolfe DE, et al. Influence of processing on the microstructural evolution and multiscala hardness in titanium carbonitrides (TiCN) produced via field assisted sintering technology. *Mater (Oxf)* 2023;vol. 27:101682. <https://doi.org/10.1016/j.mta.2023.101682>.
- [33] Chicardi E, et al. Toughening of complete solid solution cermets by graphite addition. *Chem Eng J* 2015;vol. 267:297–305. <https://doi.org/10.1016/j.cej.2015.01.022>.
- [34] Zackrisson J, Andrén H-O. Effect of carbon content on the microstructure and mechanical properties of (Ti, W, Ta, Mo)(C, N)-(Co, Ni) cermets. *Int J Refract Met Hard Mater* 1999;vol. 17(4):265–73. [https://doi.org/10.1016/S0263-4368\(98\)00074-2](https://doi.org/10.1016/S0263-4368(98)00074-2).
- [35] Akinribide OJ, et al. The role of graphite addition on spark plasma sintered titanium nitride. *J Mater Res Technol* 2020;vol. 9(3):6268–77. <https://doi.org/10.1016/j.jmrt.2020.03.040>.
- [36] Abdelbary A, Chang L. Introduction to engineering tribology. in *Principles of Engineering Tribology*. Elsevier,; 2023. p. 1–32. <https://doi.org/10.1016/B978-0-323-99115-5.00013-X>.
- [37] Verma V, Manoj Kumar BV. Tribological characteristics of conventionally sintered TiCN-WC-Ni/Co cermets against cemented carbide (Part A) *Ceram Int* 2017;vol. 43(1):368–75. <https://doi.org/10.1016/j.ceramint.2016.09.167>.
- [38] Liu J, et al. Formation of self-lubricant surface layer on the Ti(C, N)-based cermets. *Vacuum* 2017;vol. 143:225–8. <https://doi.org/10.1016/j.vacuum.2017.06.024>.
- [39] Kang X, He Y, Lin N, Zhang M, Yan Y, Huang J. A study of the preparation and properties of dense binderless titanium carbonitride-based ceramics. *J Alloy Compd* 2020;vol. 843:155941. <https://doi.org/10.1016/j.jallcom.2020.155941>.
- [40] Ji W, Zou B, Liu Y, Huang C, Guo P. Frictional behavior and wear resistance performance of gradient cermet composite tool materials sliding against hard materials. *Ceram Int* 2017;vol. 43(10):7816–26. <https://doi.org/10.1016/j.ceramint.2017.03.096>.
- [41] Verma V, Manoj Kumar BV. Tribological behavior of TiCN based cermets against steel and cemented carbide (Part B) *Mater Today Proc* 2016;vol. 3(9):3130–6. <https://doi.org/10.1016/j.matpr.2016.09.029>.
- [42] Manoj Kumar BV, Basu B. Fretting Wear Properties of TiCN-Ni Cermets: Influence of Load and Secondary Carbide Addition. *Metall Mater Trans A* 2008;vol. 39(3): 539–50. <https://doi.org/10.1007/s11661-007-9446-5>.
- [43] Prabhu TR. Effects of solid lubricants, load, and sliding speed on the tribological behavior of silica reinforced composites using design of experiments. *Mater Des* 2015;vol. 77:149–60. <https://doi.org/10.1016/j.matdes.2015.03.059>.
- [44] Hvizdoš P, Balko J, Fides M, Chicardi E. Wear damage of TiTaCN-Co cermets at room and elevated temperatures. *Procedia Struct Integr* 2017;vol. 5:1385–92. <https://doi.org/10.1016/j.prostr.2017.07.202>.
- [45] Verma V, Kumar BVM. Sliding wear behavior of SPS processed TaC-containing Ti (CN)-WC-Ni/Co cermets against Silicon Carbide. *Wear* 2017;vol. 376–377:1570–9. <https://doi.org/10.1016/j.wear.2017.02.013>.
- [46] Vettivel SC, Selvakumar N, Narayanasamy R, Leema N. Numerical modelling, prediction of Cu-W nano powder composite in dry sliding wear condition using response surface methodology. *Mater Des* 2013;vol. 50:977–96. <https://doi.org/10.1016/j.matdes.2013.03.072>.
- [47] Yang K, Basem S, El-Haik B. *Design for six sigma*. New York: McGraw-Hill; 2003.
- [48] Olorundaisi E, Jamiru T, Adegbola TA, Ogunbiyi OF. Modeling and optimization of operating parameters using RSM for mechanical behaviour of dual phase steels. *Mater Res Express* 2019;vol. 6(10):105628. <https://doi.org/10.1088/2053-1591/ab430e>.
- [49] LAKSHMINARAYANAN AK, BALASUBRAMANIAN V. Comparison of RSM with ANN in predicting tensile strength of friction stir welded AA7039 aluminium alloy joints. *Trans Nonferrous Met Soc China* 2009;vol. 19(1):9–18. [https://doi.org/10.1016/S1003-6326\(08\)60221-6](https://doi.org/10.1016/S1003-6326(08)60221-6).